RSC Advances

PAPER

View Article Online
View Journal | View Issue

Cite this: *RSC Adv.*, 2017, **7**, 32536

Evaluation of red and near infrared fluorescent silver nanoclusters as potential *in vivo* indicators of tight junction opening†

Xinyi Wang,‡[a] Na Wang,‡[c] Limei Li,[a] Ruyue Xiao,[b] Lan Yuan,[b] Xiaoda Yang *[b] and Na Li[d]

Received 17th May 2017
Accepted 19th June 2017

DOI: 10.1039/c7ra05561g

rsc.li/rsc-advances

Tight junctions (TJs) play a key role in regulating permeability to liquids, ions and larger solutes through the paracellular route. To demonstrate TJ structure changes by measuring paracellular flux is challenging for understanding biological functions of tight junction and designing delivery system for highly hydrophilic macromolecular drugs. In the present study, we tested two long wavelength emitting silver nanoclusters (AgNCs), Ag_2S(BSA)-NCs ($\lambda_{ex/em}$ at 500/1050 nm) and Ag(GSH)-NCs ($\lambda_{ex/em}$ at 488/640 nm), for their suitability as novel paracellular permeation indicators on a MDCK monolayer. Ag_2S(BSA)-NCs exhibited marginal cytotoxicity and passed through the cell monolayer exclusively *via* the paracellular pathway. However, Ag(GSH)-NCs could be taken inside the cells possibly through endocytosis. AgNCs together with Eu-DTPA were used in the double probe strategy for detecting the change of TJ pore path parameters (*i.e.* pore size r and retention capacity ε/τ) upon TJ opening with EDTA or vanadyl acetylacetonates, respectively. The AgNCs/Eu-DTPA probe set was found to give the same results as our previous work using the short wavelength emitting AuNCs and Eu-DTPA probe set, suggesting future potential applications of AgNCs to the *in vivo* studies of TJ alternations upon stresses. This work reinforced the use of a double probe set for study of the TJ structure change.

Introduction

The tight junction (TJ) indicates the intercellular junctional complex located at the apical-most portion of epithelial cell monolayers. The TJ forms one major mechanism for restricting or regulating passage of liquids, ions, and large solutes through the paracellular pathway.[1–3] TJ structures are composed of a variety of proteins including trans-membrane proteins, cytoskeletal proteins, scaffolding components, regulatory and signaling molecules.[4,5] These proteins are deliberately arranged for integrating biological barriers as well as fabricating a complex signaling network.[6,7] Various physiological and/or pathological events can alter TJ structures and functions, *e.g.* the salivary gland and some endothelial cell secretion,[8,9] the metabolite (*e.g.* amyloid-β) clearance from the brain *via* the blood–brain barrier (BBB),[10,11] inflammatory mediator-induced changes in paracellular permeability[12,13] and toxicity of metal ions.[14,15] In addition, the rational drug delivery system with additional adjusting TJ opening design have been an important approach for drug delivery through biological barriers.[16–20]

Thence, methods that help to characterize the TJ architecture and properties of paracellular pathways would be crucial for studies of the mechanism of TJ regulations and related pharmacological applications described above. TJ architecture observation can be realized using some techniques and methods, *e.g.* electron microscopy using the freeze-fracture technique is a valid means for observing the ultrastructures of TJ,[21,22] and fluorescence microscopy with genetically encoded fluorescent proteins realizes dynamic imaging of TJ for studying their dynamic nature in living cells.[23,24] However, these methods lack the paracellular permeability assessment. The trans-epithelial electrical resistance (TEER) measurement is an indirect means for scaling paracellular permeability.[25,26] The pore size as a important index of paracellular permeability is usually scaled using various sized paracellular permeation probe/markers, most of which need radioactive or fluorescent labeling.[27–31] It is always desired to realize real timely monitoring of the paracellular permeability of TJ. Previously, we developed a feasible methods utilizing double

[a]*College of Sciences, Shenyang Agricultural University, Shenyang 110161, China*
[b]*State Key Laboratory of Natural and Biomimetic Drugs, Department of Chemical Biology, School of Pharmaceutical Sciences, Peking University, Beijing 100083, China. E-mail: xyang@bjmu.edu.cn; Fax: +86-10-62015584; Tel: +86-10-82801539*
[c]*Department of Pharmacognosy, School of Pharmaceutical Sciences, Hebei Medical University, Shijiazhuang 050017, China*
[d]*Beijing National Laboratory for Molecular Sciences (BNLMS), The Key Laboratory of Bioorganic Chemistry and Molecular Engineering, Ministry of Education, College of Chemistry and Molecular Engineering, Peking University, Beijing 100871, China*

† Electronic supplementary information (ESI) available: Characterization of AgNCs; TEER stability of MDCK cell monolayer treated with AgNCs; TJ mediation treated by EDTA and $VO(acac)_2$; size exclusion chromatography of Eu-DTPA and AgNCs. See DOI: 10.1039/c7ra05561g

‡ Xinyi Wang and Na Wang contributed equally to this work

fluorescent probe combination of Eu-DTPA with fluorescent gold nanoclusters (AuNCs) to observe the dynamic alteration of TJ pore size (r) and retention parameters (ε) upon the treatment with drugs and/or stimuli.[32] This shed lights on the application of ultra-fine fluorescent nanoclusters in detecting the properties of paracellular pathways. Compared with AuNCs, the silver nanoclusters (AgNCs) are more readily prepared with brighter fluorescence emission (higher quantum yield).[33,34] Additionally, AgNCs possess the second near-infrared (NIR-II) fluorescence emission that is optimal for optical imaging of living animals due to much lower albedo and endogenous autofluorescence.[35] Thence, AgNCs may be potentially better *in vivo* paracellular permeation indicators over AuNCs.

In light of this, we in this effort explored the feasibility of naturally occurring biomolecules, bovine serum albumin (BSA) and glutathione (GSH) templated AgNCs for studying the TJ changes. For the selection of ligands, some essential elements need to be considered involving biocompatibility, considerable difference in volumes and surface negative charges *etc.* We first prepared two long wavelength excitation/emission AgNCs, *i.e.* BSA-stabilized Ag_2S(BSA)-NCs ($\lambda_{ex/em}$ at 500/1050 nm) and GSH-protected Ag(GSH)-NCs ($\lambda_{ex/em}$ at 488/640 nm). We evaluated the cytotoxicity and clarifying their permeation pathways across the MDCK cell monolayers. Then the AgNCs/Eu-DTPA double probe strategy was applied to measure the change of the TJ pore size (r) and retention parameters upon treatment of two different TJ openers on a MDCK cell monolayer model. The MDCK cell monolayer represents a well-established model for the study of permeability and toxicity of drugs across biological barriers.[36] The results showed that the AgNCs/Eu-DTPA probe sets gave identical results with the previous AuNCs/Eu-DTPA probes, reinforcing the applicability of the double probe strategy to TJ study by combining the subnanometer long wavelength emitting AgNCs with the long luminescence lifetime Eu-DTPA and suggesting potential applications to studies *in vivo* in the future.

Experimental

Materials

MDCK (Madin-Darby canine kidney) cell was purchased from Institute of Materia Medica, Chinese Academy of Medical Sciences, Beijing. Dulbecco's Modified Eagle's Medium (DMEM), penicillin–streptomycin and fetal bovine serum (FBS) were sourced from GIBCO, Invitrogen Corp. (Carlsbad, CA, USA). Transwell plates (12 wells, pore diameter of 3 μm, polycarbonate) were purchased from Corning Costar (Cambridge, MA). Eu_2O_3 (99.99%), potassium hydrogen phthalate, and diethylene triamine pentaacetic acid (DTPA) were purchased from Sinopharm Chemical Reagent Corp (Beijing). Trioctyl phosphine oxide (TOPO) was purchased from Sigma-Aldrich (St. Louis, MO, USA). The MTS tetrazolium compound was purchased from Promega Corp. (Madison, WI, USA). All the other reagents were of analytical grade from commercial source.

Synthesis of silver nanoclusters

BSA-stabilized AgNCs (denoted as Ag_2S(BSA)-NCs) were prepared according to the previously reported procedure.[37] Briefly, 50 mL BSA nitrate (2 mmol L^{-1}) and 25 mL silver nitrate solution (4 mmol L^{-1}) hybrid solution were mixed and vigorous stirred for 24 h, then 25 mL Na_2S (8 mmol L^{-1}, speed 480 μL min^{-1}) were added. The synthetic products were Ag_2S fluorescence nanocluster which template as BSA (Ag_2S(BSA)-NCs). The concentration of Ag_2S(BSA)-NCs solution was quantified using ICP-MS (NexION 300X, Perkin Elmer, USA) after purification by dialysis and stored at 4 °C.

GSH-stabilized AgNCs, denoted as Ag(GSH)-NCs, were prepared according to the previously reported procedure.[35] Briefly, $AgNO_3$ aqueous solution (125 μL, 20 mM) were mixed with GSH aqueous solution (5 mL, 1.5 mM) under vigorous stirring to form the Ag(I)–GSH complexes. Then, $NaBH_4$ solution (50 μL, 112 mM) was added and a deep-red AgNCs solution was obtained. After another 3 h incubation until the disappearance of deep-red color, another 50 μL of $NaBH_4$ solution was added for another incubation of 8 h at room temperature. Eventually, the brown AgNC solution was obtained. Ag(GSH)-NCs were purified using a dialysis bag with a molecular weight cut off (MWCO) of 1 kDa.

Preparation of Eu-DTPA probe

Eu-DTPA complexes were prepared using the previous method.[32] Briefly, 0.01 mol L^{-1} $EuCl_3$ solution were added dropwise into 0.01 mol L^{-1} DTPA solution in Hank's balanced salt solution (HBSS; pH 7.0) until appearing a white cloudy sediment, then the supernatant (Eu-DTPA) was collected after centrifuge (3 min, 10 000 × g).

Preparation of non-fluorescence DMEM medium (NF-DMEM)

To prevent the interference of autofluorescence background in DMEM media, some amino acids (tryptophan, tyrosine, and phenylalanine) and vitamins (folic acid, pyridoxine hydrochloride, and riboflavin) were excluded referring to GIBCO™ catalogue media formulations when preparing the non-fluorescence DMEM media (NF-DMEM). The fluorescence-free DMEM media did not show any influences on MDCK cell viability or tight junction formation of MDCK cell monolayer.

MDCK cell culture

MDCK cells were cultured in sterile, vented 25 cm^2 cell culture flasks with high glucose DMEM supplemented with 10% (v/v) FBS and double antibiotics (100 U penicillin and 100 μg mL^{-1} streptomycin) in a humidified incubator (37 °C and 5% CO_2). The medium was refreshed every 2 days. Cells were passaged at 70–90% confluency using 0.25% (w/v) trypsin–0.02% (w/v) ethylene diamine tetraacetic acid (EDTA) solution. The MDCK cells used in this study were under passage 50.

Cytotoxicity assay

Toxicity of AgNCs on MDCK cells was estimated by MTS assay using a CellTiter 96® AQueous One Solution Cell Proliferation

Assay kit (Promega Inc., Madison, WI). In brief, MDCK cells (3–5 $\times$ 10^3 cells per mL) were seeded in 96 well plates (200 μL per well). After attaching on the wall of plates, the cells were incubated with various concentrations of AgNCs in DMEM for 3, 6, 12, and 24 h. Then the cells were rinsed with DMEM and incubated with MTS solution for another 3 h at 37 °C. The absorbance of the color development in AgNCs-treated and untreated cells was measured in a Bio-Rad Microplate reader using 570 nm as the detection wavelength.

Transport experiment and P_{app} calculation

MDCK monolayers were seeded on transwell filters (aperture, 3 μm; diameter, 1.12 cm). After plating cells on filters (1–5 $\times$ 10^4 cells per well), the medium was replaced every 24 h until 5–7 days when the net trans-epithelial electrical resistance (TEER) exceeded 200 Ω cm. For the trans-epithelial transport experiments, the MDCK monolayers were rinsed twice with warm NF-DMEM media (37 °C). Then different concentrations of Eu-DTPA and/or AgNCs in NF-DMEM media were added to the apical chamber and samples were taken from the basolateral chamber at different time intervals. The apparent permeability coefficients (P_{app}) of Eu-DTPA/AgNCs were calculated by the formula $P_{app} = (\Delta Q/\Delta t)/(AC_0)$, where A is the surface area of the inserts (1.13 cm^2 in this study), C_0 is the initial concentration of Ag_2S(BSA)-NCs (mg mL^{-1}) in the apical chamber.

The concentration of Eu-DTPA was detected by a time-resolved fluorescence assay. Briefly, the samples and $EuCl_3$ standard (0–80 nM) were mixed at a ratio of 1 : 1 (v/v) with two-fold enhancement solution (30 μmol L^{-1} β-NTA, 10 mmol L^{-1} TOPO, 0.2% Triton X-100, and 0.1 mol L^{-1} potassium hydrogen phthalate buffer (pH 3.0)) and left at room temperature for 1 h. The fluorescence intensity was measured on a Flexstation 3 microplate reader with an $\lambda_{ex/em}$ of 340/616 nm and a measurement window from 600 to 1000 ms.

The concentration of AgNCs was determined by fluorescence assays. The fluorescence spectroscopy of Ag_2S(BSA)-NCs was obtained with a Hitachi F4600 spectrophotometer (Hitachi, Japan). The fluorescent intensity of AgNCs samples from the basolateral chamber were detected on a Flexstation 3 microplate reader with an ex/em of 500/1050 nm for Ag_2S(BSA)-NCs and 488/630 nm for Ag(GSH)-NCs.

Treatment of MDCK monolayers with EDTA or vanadyl acetylacetonate ($VO(acac)_2$)

For the paracellular diffusion, permeability of solutes would be greatly improved when the TJ structure was opened or destroyed. In order to test the indication of permeability alternation by AgNCs and Eu-DTPA double probes, we chose EDTA and vanadium complexes as TJ opening mediators. EDTA and its analogues have been widely used to disrupt reversibly TJ proteins by depleting Ca^{2+} and Mg^{2+} ions which result in a high paracellular permeability of hydrophilic macromolecules;[38] vanadium complexes can damage TJs through inducing oxidative stress, resulting in a relatively lower paracellular permeability.[39] Hereby, the influence of EDTA and vanadium complexes on MDCK cell monolayer were investigated by including 0.5 mmol L^{-1} of EDTA or 80 μmol L^{-1} of $VO(acac)_2$ in the Ca^{2+} and Mg^{2+} free NF-DMEM in the transport experiments described above (Fig. S6†).

Estimation of D_p values through P_{app} values

The P_{app} values are proportional to the D_p values as described by the following equation:

$$P_{app} = D_p \frac{K_{m/f}}{h} = aD_p \quad (1)$$

where h is thickness of the membrane and $K_{m/f}$ is a constant for the membrane. Considering that under the condition of complete opening of tight junction (*i.e.* after treatment with 0.5 mmol L^{-1} EDTA), D_p would tend to be close to D_{AB_p}. Therefore, the scale factor a for a certain fluorescent probe can be estimated by the following equation:

$$a = \frac{P_{app,max}(\text{TJ fully opening})}{D_{AB}} \quad (2)$$

Then, the D_p values are estimated by the following equation:

$$D_p = \frac{P_{app}}{a} \quad (3)$$

Calculation of the pore size and the retention capacity of tight junction upon TJ opening

Given that the diffusion of the probes in tight junction channels is similar to that in porous medium and there is no specific interaction among the solutes, solvents and tight junction channels, diffusion of the probes could be described by the amended Knudsen equation:

$$D_p = \left(\frac{1}{D_{AB_p}} + \frac{1}{D_{K_p}}\right)^{-1} \quad (4)$$

in which

$$D_{AB_p} = D_{AB}\frac{\varepsilon}{\tau}, \quad D_{K_p} = kr\left(\frac{T}{M_A}\right)^{1/2} \quad (5)$$

where D_{AB_p} is the diffusion coefficient of probes in solvent B; ε and τ represent porosity and tortuosity of the porous medium, respectively; r is the radius of the pore; M_A is the molecular mass of the solute. The ε/τ is in overall reflecting the retention capacity of the porous medium on the solutes. Considering the size exclusion effect, ε/τ is thus different among the Eu-DTPA and AgNCs. We assume that the large AgNC probes only pass through the large pores and their ε/τ is assigned as the intrinsic one. Therefore, the ε/τ factor for Eu-DTPA would be described by

$$(\varepsilon/\tau)_{\text{Eu-DTPA}} = (\varepsilon/\tau) \times 10^{t_r(\text{Eu-DTPA})/t_r(\text{AgNCs})} \quad (6)$$

where the retention time (t_r) of the probes was measured on a size exclusion gel column (*e.g.* Sephadex G25, see Fig. S7†). Then, the Knudsen equations for the three fluorescent probes were obtained as:

$$\frac{1}{D_p}(\text{Eu-DTPA}) = 1.02 \times 10^{11}\frac{\tau}{\varepsilon} + 1.37\frac{1}{k}\frac{1}{r} \quad (7)$$

$$\frac{1}{D_p}(\text{Ag(GSH)-NCs}) = 6.94 \times 10^{10}\,\frac{\tau}{\varepsilon} + 3.89\,\frac{1}{k}\,\frac{1}{r} \quad (8)$$

$$\frac{1}{D_p}(\text{Ag}_2\text{S(BSA)-NCs}) = 1.76 \times 10^{10}\,\frac{\tau}{\varepsilon} + 19.77\,\frac{1}{k}\,\frac{1}{r} \quad (9)$$

By assigning the size ($r \sim 4$ Å) of primary TJ pores[40] as the average size of TJ pores, the calibration constant was calculated to be 0.139 ± 0.053. Then, the change of pore size (r) and retention capacity (ε/τ) could be calculated using the following two sets of equations:

- When using Eu-DTPA + AgNC(GSH)-NCs:

$$\frac{1}{D_p}(\text{Eu-DTPA}) = 1.02 \times 10^{11}\,\frac{\tau}{\varepsilon} + 9.856\,\frac{1}{r} \quad (10)$$

$$\frac{1}{D_p}(\text{Ag(GSH)-NCs}) = 6.94 \times 10^{10}\,\frac{\tau}{\varepsilon} + 27.98\,\frac{1}{r} \quad (11)$$

- When using Eu-DTPA + Ag_2S(BSA)-NCs:

$$\frac{1}{D_p}(\text{Eu-DTPA}) = 1.02 \times 10^{11}\,\frac{\tau}{\varepsilon} + 9.856\,\frac{1}{r} \quad (12)$$

$$\frac{1}{D_p}(\text{Ag}_2\text{S(BSA)-NCs}) = 1.76 \times 10^{10}\,\frac{\tau}{\varepsilon} + 142.23\,\frac{1}{r} \quad (13)$$

ICP-MS quantification of the cellular uptake

When the cell growth reached nearly 90% confluence (in the 6 well microplate), the Eu-DTPA and AgNC probe solution were added to the cultivation media at the desired concentrations at 37 °C (10% FBS) or 25 °C (free FBS). After 6 h of incubation, cells were washed, trypsinized and collected. The samples were treated with aqua regia overnight to dissolve the cells and the Ag particles. Then the samples were analyzed with the ICP-MS (NexION 300X, PerkinElmer, USA) to measure the amount of silver atoms per cell.

Statistics

Means of at least three replicates per treatment were shown as data points for each parameter of study. Analysis of data was carried out by *t*-test or one-way analysis of variance (ANOVA). A *P*-value less than 0.05 was considered as statistically significant.

Results and discussion

Synthesis and characterization of AgNCs

Ag_2S(BSA)-NCs and Ag(GSH)-NCs were prepared as described previously.[35,37] Characterization using fluorescence, transmission electron microscope (TEM), Fourier transform infrared (FT-IR) spectroscopy, and the dynamic light scattering (DLS) (Fig. S1–S3,† and Table 1) demonstrated that desired products were obtained. Both AgNCs showed similar core particle size of ~2.8 nm (Fig. 1), Ag_2S(BSA)-NCs exhibited obviously larger hydrodynamic diameter than Ag(GSH)-NCs (Table 1). Based on the fluorescent graphs (Fig. S4†), we chose $\lambda_{ex/em}$ of 500/1050 nm and 488/640 nm for following determinations of Ag_2S(BSA)-NCs and Ag(GSH)-NCs, respectively.

Cytotoxicity of AgNCs on MDCK cells

The cytotoxicity of AgNCs on MDCK cells were estimated by MTS assays and TEER measurements. Ag_2S(BSA)-NCs (0–128 mg L^{-1}) was shown to impart no significant effects on cell viability (Fig. 2). Ag(GSH)-NCs (0–8 mg L^{-1}) did not affect cell viability within 6 h incubation, however, slightly decreased cell growth over 12 h or longer incubation. In addition, neither caused any decline of transepithelial electric resistance (TEER) in 10 h incubation (Fig. S5†). Nevertheless, these results indicated that AgNCs were not toxic to MDCK cells in the 4 h transportation assays.

Mechanism of AgNCs permeation through MDCK monolayer

To clarify the mechanism of membrane permeation of AgNCs, the values of the apparent permeability coefficient (P_{app}) and the rates of cellular accumulation were determined and the results were shown in Table 2. It is noted that Ag_2S(BSA)-NCs exhibited the P_{app} value lower than 10^{-6} cm s^{-1} and almost no cellular retention, indicating paracellular pathway for Ag_2S(BSA)-NCs according to the criteria for paracellular markers.[41] The P_{app} of Ag_2S(BSA)-NCs is even much smaller than that of typical paracellular marker Eu-DTPA, the reason is obvious that Ag_2S(BSA)-NCs has much larger size, and thus much smaller diffusion rate ($D_{AB_p} = 3.36 \times 10^{-10}$ for Eu-DTPA).[32,39] However, Ag(GSH)-NCs exhibited very high rate of cellular accumulation, regardless the comparable P_{app} as that of Eu-DTPA, suggesting

Table 1 Some physicochemical parameters of AgNCs

Parameters	Ag_2S(BSA)-NCs	Ag(GSH)-NCs
M_A (g mol^{-1})	11.65×10^4	4.5×10^3
Particle core diameter (nm) (TEM)	2.7 ± 0.8	2.9 ± 0.9
Volume weighted hydrodynamic diameter (nm)	11.8 ± 5.2	5.0 ± 2.6
ζ potential (mV)	−24.0 ± 6.8	−17.6 ± 6.3
D_{AB}[a] (m^2 S^{-1})	5.67×10^{-11}	1.68×10^{-10}

[a] Parameters calculated using the Polson's equation: $D_{AB} = \frac{9.4 \times 10^{-15} T}{\mu_B (M_A)^{1/3}}$, where V_A is the volume of solute probe; μ_B and M_A are the viscosity and molar mass of the solvent water, respectively; T is the absolute temperature.

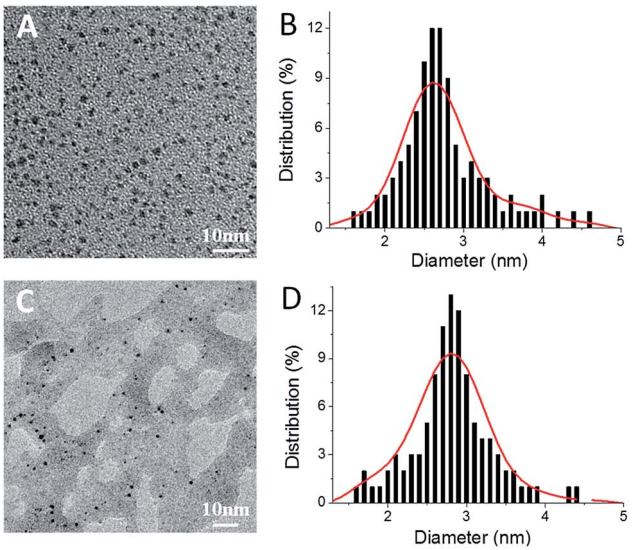

Fig. 1 TEM images of Ag_2S(BSA)-NCs (A) and Ag(GSH)-NCs (C). Histograms of (B) and (D) show the size distribution of Ag_2S(BSA)-NCs and Ag(GSH)-NCs obtained from corresponding TEM image ($n = 100$), respectively.

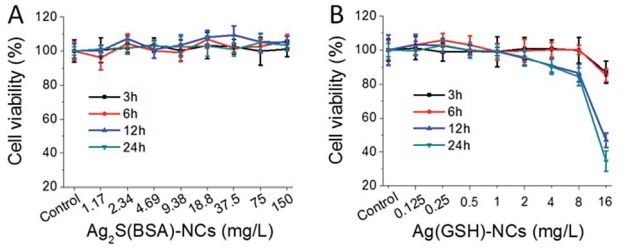

Fig. 2 MTS assays of MDCK cells upon treatment with AgNCs. (A) Ag_2S(BSA)-NCs. (B) Ag(GSH)-NCs. All data were the mean ± SD of four replicates.

that Ag(GSH)-NCs should pass through the cell monolayer *via* both paracellular and transcellular pathways.

The different mechanisms for cell monolayer membrane transport with two types of AgNCs might be attributed to the different chemical species of Ag in the nanocluster. In Ag_2S(BSA)-NCs, Ag^+ ions form stable coordination bonds with S^{2-} and thus no longer active; while in Ag(GSH)-NCs, GSH only bind to part of the surface Ag atoms and provide ζ potential. Thence, the Ag atom in nanoparticles could still interact with certain biological molecules of the cell and cause subsequences, *e.g.* transcytosis and release of Ag^+ in presence of oxygen.[42] This may explain the cytotoxicity of Ag(GSH)-NCs upon 12 h or longer incubation.

Alternations of TJ pore size and retention capacity with Eu-DTPA and Ag_2S(BSA)-NCs double probes

Alternation of TJ pore size and retention capacity upon opening with EDTA was investigated by using Eu-DTPA and Ag_2S(BSA)-NCs as double paracellular diffusion probes as described.[32,39] The results (Fig. 3) showed that upon EDTA treatment, P_{app} of

Table 2 The P_{app} and rates of cellular accumulation of AgNCs in MDCK cells

Compound	P_{app} ($\times 10^{-7}$ cm^{-1})	Cellular accumulation[a] (%)
Eu-DTPA	1.50 ± 0.10	n.a
Ag_2S(BSA)-NCs	0.23 ± 0.10	0.06 ± 0.03
Ag(GSH)-NCs	2.5 ± 1.7	2.86 ± 0.09

[a] Cell incubated with AgNCs for 6 h at 25 °C in FBS-free DMEM media. Accumulation rate is calculated by dividing the AgNCs concentration in cell monolayer by the AgNCs concentration in cultural media.

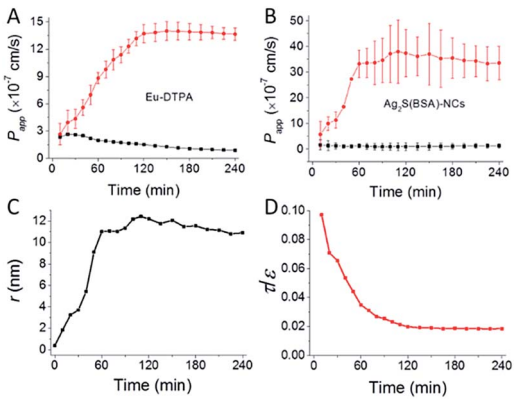

Fig. 3 The time course of membrane permeation of Eu-DTPA (A) and Ag_2S(BSA)-NCs (B) probes with (cycle) or without (square) EDTA (0.5 mmol L^{-1}) treatment. (C) and (D) shows the change of tight junction pore size (r) and retention capacity (ε/τ) calculated based on data in (A) and (B) as described previously.[32] Eu-DTPA (20 μmol L^{-1}) and Ag_2S(BSA)-NCs (75 mg L^{-1}) were added in the apical side of MDCK monolayer and samples was collected in the basolateral side for P_{app} determination as described in Experimental section. Data were the mean ± SD of three replicates.

both probes increased along incubation time until reaching a plateau (Fig. 3A and B); while the calculation indicated that TJ pores were enlarged to a radius value about ~12 nm and the retention capacity (ε/τ) decreased continually to a stable value (Fig. 3C and D), indicating formation of smooth intercellular channels. The present result agrees well with the characteristic of TJs disrupted by Ca^{2+} chelating agent,[38,40,43,44] as well as our previous determinations using the AuNCs/Eu-DTPA system.[32]

Results of membrane permeation of the double fluorescent probes upon treatment with vanadyl complexes are shown in Fig. 4. Different from Eu-DTPA, no obvious changes of P_{app} of Ag_2S(BSA)-NCs were observed. This result demonstrated that TJ pores caused by vanadium treatment must be less than 12 nm in radius. However, this data set precluded further calculation of TJ pore parameters.

Ag(GSH)-NCs exhibited both paracellular and transcellular pathways. However, as the overall P_{app} (2.5×10^{-7} cm^{-1}) is low, the transcellular permeation background should be very limited. Thence, we were able to observe the effect of vanadyl complexes on permeation of Ag(GSH)-NCs. As shown in Fig. 5A, P_{app} of Ag(GSH)-NCs increased upon vanadium treatment in

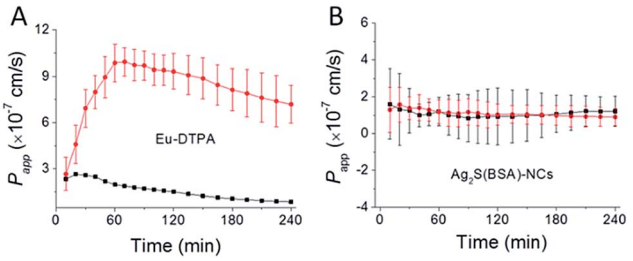

Fig. 4 The time course of membrane permeation of Eu-DTPA (A) and Ag_2S(BSA)-NCs (B) probes with (cycle) or without (square) vanadyl acetylacetonate (80 μmol L^{-1}) treatment. Eu-DTPA (20 μmol L^{-1}) and Ag_2S(BSA)-NCs (75 mg L^{-1}) were added in the apical side of MDCK monolayer and samples was collected in the basolateral side for P_{app} determination as described in Experimental section. Data were the mean ± SD of three replicates.

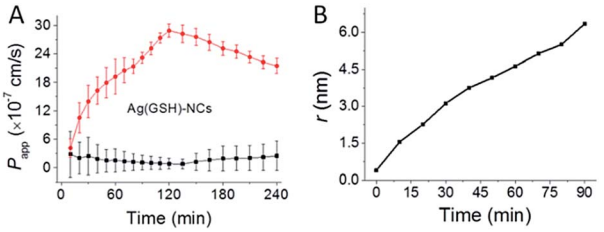

Fig. 5 The time course of membrane permeation of Ag(GSH)-NCs (A) probes with (cycle) or without (square) vanadyl acetylacetonate (80 μmol L^{-1}) treatment. (B) shows the change of tight junction pore size (*r*) calculated based on data in (A). Ag (GSH)-NCs (8 mg L^{-1}) were added in the apical side of MDCK monolayer and samples was collected in the basolateral side for P_{app} determination as described in Experimental section. Data were the mean ± SD of three replicates.

a multiple phasic permeation process. The first period of permeability increase (90 min) is obviously associated with the vanadium-induced TJ opening. Increase of permeability later on might be attributed to the Ag toxicity on cytoplasmic membrane of MDCK cells following the endocytosis of Ag nanoparticles, as it was demonstrated previously that AgNCs caused breakage of cytoplasmic membrane through releasing of Ag^+.[42,45] Thence, the permeability data set within 90 min with vanadium treatment could be applied to estimate the change of TJ pore paths. As shown in Fig. 5B, upon vanadium treatment, the radius of TJ pore increased gradually to a maximal size expected to be 6–7 nm, which is again in good consistence with our previous observation (~6 nm) obtained with AuNCs/Eu-DTPA double probes.[32]

The dynamic changes of TJ pore path parameters upon chemical stresses have first been measured using the AuNCs/Eu-DTPA double probes.[32] Herein, results from the new AgNCs/Eu-DTPA probe sets reinforced the results obtained with the AuNCs/Eu-DTPA double probes. The present work, together with our previous work, solidifies that the double fluorescence probe strategy is a practical approach for investigation of tight junction structural alternations. Moreover, the success of present application *in vitro* should suggest future potential application of AgNCs *in vivo* studies by taking advantage of the long excitation/emission wavelength of AgNCs.

Our results also suggested that a few important issues need to be addressed before *in vivo* applications of AgNCs for detecting TJ structure alternations: (i) possibly due to the interaction of albumin with TJ proteins, Ag_2S(BSA)-NCs (as well as Au@BSA-NCs) could only reveal the TJ pore size up to ~12 nm. To overcome this limitation, new stabilizing agents other than albumin should be tested for developing more neural fluorescent Au/Ag_2S nanoclusters; (ii) GSH-protected Ag nanocluster unexpectedly showed metal toxicity on cells and TJ. New synthetic methods or protecting agents should be investigated to prepare fully protected Ag^0 nanoclusters.

Conclusions

The present work evaluated red and near infrared fluorescent silver nanoclusters, *i.e.* Ag_2S(BSA)-NCs and Ag(GSH)-NCs, as novel indicators for monitoring the alteration of the TJ structure upon stresses, *e.g.* EDTA or vanadyl acetylacetonates treatment. The results using AgNCs/Eu-DTPA probe sets reinforced the previous findings using AuNCs/Eu-DTPA probes. Taking advantage of the long wavelength excitation/emission of AgNCs, our results indicated future potential applications of AgNCs to the *in vivo* studies of TJ pore size and structural properties and the alternations upon stresses after further improving the surface modification and stability of the metal nanoclusters. Nonetheless, future works using AgNCs to demonstrate *in vivo* TJ alterations related to physiological/pathological conditions would be expected soon.

Acknowledgements

This work was supported by National Natural Science Foundation of China (No. 21271012; 31571025).

References

1 J. L. Madara, *Annu. Rev. Physiol.*, 1998, **60**, 143–159.
2 C. Guillot and T. Lecuit, *Science*, 2013, **340**, 1185–1189.
3 U. Kniesel and H. Wolburg, *Cell. Mol. Neurobiol.*, 2000, **20**, 57–76.
4 S. Tsukita, M. Furuse and M. Itoh, *Nat. Rev. Mol. Cell Biol.*, 2001, **2**, 285–293.
5 L. Gonzalez-Mariscal, A. Betanzos, P. Nava and B. E. Jaramillo, *Prog. Biophys. Mol. Biol.*, 2003, **81**, 1–44.
6 D. Mehta and A. B. Malik, *Physiol. Rev.*, 2006, **86**, 279–367.
7 L. Gonzalez-Mariscal, R. Tapia and D. Chamorro, *Biochim. Biophys. Acta, Biomembr.*, 2008, **1778**, 729–756.
8 D. A. D. Nguyen and M. C. Neville, *J. Mammary Gland Biol. Neoplasia*, 1998, **3**, 233–246.
9 P. Ewert, S. Aguilera, C. Alliende, Y.-J. Kwon, A. Albornoz, C. Molina, U. Urzua, A. F. G. Quest, N. Olea, P. Perez, I. Castro, M.-J. Barrera, R. Romo, M. Hermoso, C. Leyton and M.-J. Gonzalez, *Arthritis Rheum.*, 2010, **62**, 1280–1289.
10 S. W. Park, J. H. Kim, S. M. Park, M. Moon, K. H. Lee, K. H. Park, W. J. Park and J. H. Kim, *Oncotarget*, 2015, **6**, 35263–35273.

11 J. D. Huber, R. D. Egleton and T. P. Davis, *Trends Neurosci.*, 2001, **24**, 719–725.
12 B. V. Zlokovic, *Neuron*, 2008, **57**, 178–201.
13 N. J. Abbott, *Cell. Mol. Neurobiol.*, 2000, **20**, 131–147.
14 J. Das, M. H. Kang, E. Kim, D. N. Kwon, Y. J. Choi and J. H. Kim, *Sci. Rep.*, 2015, **5**, 13921.
15 A. R. Calabro, D. I. Gazarian and F. A. Barile, *J. Pharmacol. Toxicol. Methods*, 2011, **63**, 47–58.
16 G. Miller, *Science*, 2002, **297**, 1116–1118.
17 Y. Chen and L. Liu, *Adv. Drug Delivery Rev.*, 2012, **64**, 640–665.
18 N. N. Salama, N. D. Eddington and A. Fasano, *Adv. Drug Delivery Rev.*, 2006, **58**, 15–28.
19 I. Tamai and A. Tsuji, *J. Pharm. Sci.*, 2000, **89**, 1371–1388.
20 M. Amidi, E. Mastrobattista, W. Jiskoot and W. E. Hennink, *Adv. Drug Delivery Rev.*, 2010, **62**, 59–82.
21 K. J. Fujimoto, *Cell Sci.*, 1995, **108**, 3443–3449.
22 M. Furuse, H. Sasaki and S. J. Tsukita, *Cell Biol.*, 1999, **147**, 891–903.
23 T. Miyamoto, M. Furuse and M. Furutani-Seiki, *Methods Mol. Biol.*, 2011, **762**, 171–178.
24 F. K. Riesen, B. Rothen-Rutishauser and H. Wunderli-Allenspach, *Histochem. Cell Biol.*, 2002, **117**, 307–315.
25 J. Smith, E. Wood and M. Dornish, *Pharm. Res.*, 2004, **21**, 43–49.
26 B. Srinivasan, A. R. Kolli, M. B. Esch, H. E. Abaci, M. L. Shuler and J. J. Hickman, *JALA*, 2015, **20**, 107–126.
27 C. Hilgendorf, H. Spahn-Langguth, C. G. Regardh, E. Lipka, G. L. Amidon and P. Langguth, *J. Pharm. Sci.*, 2000, **89**, 63–75.
28 A. J. M. Watson, S. Y. Chu, L. Sieck, O. Gerasimenko, T. Bullen, F. Campbell, M. McKenna, T. Rose and M. H. Montrose, *Gastroenterology*, 2005, **129**, 902–912.
29 R. M. Al-Sadi and T. Y. Ma, *J. Immunol.*, 2007, **178**, 4641–4649.
30 S. P. Hong, P. R. Leroueil, E. K. Janus, J. L. Peters, M. M. Kober, M. T. Islam, B. G. Orr, J. R. Baker and M. M. B. Holl, *Bioconjugate Chem.*, 2006, **17**, 728–734.
31 T. F. Salles Teixeira, A. P. Boroni Moreira, N. C. Silva Souza, R. Frias and P. M. C. Gouveia, *Nutr. Hosp.*, 2014, **29**, 269–281.
32 X. Y. Wang, N. Wang, L. Yuan, N. Li, J. X. Wang and X. D. Yang, *Sci. Rep.*, 2016, **6**, 1–11.
33 S. X. Wang, X. M. Meng, A. Das, T. Li, Y. B. Song, T. T. Cao, X. Y. Zhu, M. Z. Zhu and R. C. Jin, *Angew. Chem., Int. Ed.*, 2014, **53**, 2376–2380.
34 S. H. Yau, B. A. Ashenfelter, A. Desireddy, A. P. Ashwell, O. Varnavski, G. C. Schatz, T. P. Bigioni and T. Goodson, *J. Phys. Chem. C*, 2017, **121**, 1349–1361.
35 H. Y. Yang, Y. W. Zhao, Z. Y. Zhang, H. M. Xiong and S. N. Yu, *Nanotechnology*, 2013, **24**, 055706.
36 N. L. Simmons, *Gen. Pharmacol.*, 1982, **13**, 287–291.
37 J. H. Xiang, H. Q. Cao, Q. Z. Wu, S. C. Zhang, X. R. Zhang and A. A. R. Watt, *J. Phys. Chem. C*, 2008, **112**, 3580–3584.
38 A. Takasawa, T. Kojima, T. Ninomiya, M. Tsujiwaki, M. Murata, S. Tanaka and N. Sawada, *Cell Tissue Res.*, 2013, **351**, 73–84.
39 Z. H. Xu, X. Y. Wang, R. Y. Xiao and X. D. Yang, *J. Chin. Pharm. Sci.*, 2013, **22**, 5.
40 L. Shen, C. R. Weber, D. R. Raleigh, D. Yu and J. R. Tumer, *Annu. Rev. Physiol.*, 2011, **73**, 283–309.
41 Y. S. Quan, K. Hattori, E. Lundborg, T. Fujita, M. Murakami, S. Muranishi and A. Yamamoto, *Biol. Pharm. Bull.*, 1998, **21**, 615–620.
42 L. Wang, T. Zhang, P. Li, W. Huang, J. Tang, P. Wang, J. Liu, Q. Yuan, R. Bai, B. Li, K. Zhang, Y. Zhao and C. Chen, *ACS Nano*, 2015, **9**, 6532–6547.
43 M. Tomita, M. Hayashi and S. Awazu, *J. Pharm. Sci.*, 1996, **85**, 608–611.
44 K. Sonaje, E. Chuang, K. Lin, T. Yen, F. Su, M. Tseng and H. Sung, *Mol. Pharmaceutics*, 2012, **9**, 1271–1279.
45 M. Ahamed, M. S. Alsalhi and M. K. J. Siddiqui, *Clin. Chim. Acta*, 2010, **411**, 1841–1848.